



Brachiation of a polymer chain in the presence of a dynamic networkPamela C. Cai ¹, Brad A. Krajina,¹ and Andrew J. Spakowitz ^{1,2,3,4}¹*Department of Chemical Engineering, Stanford University, Stanford, California 94305, USA*²*Department of Materials Science, Stanford University, Stanford, California 94305, USA*³*Department of Applied Physics, Stanford University, Stanford, California 94305, USA*⁴*Biophysics Program, Stanford University, Stanford, California 94305, USA*

(Received 2 March 2020; accepted 8 July 2020; published 6 August 2020)

The viscoelastic behavior of a physically crosslinked gel involves a spectrum of molecular relaxation processes, which at the single-chain level involve the chain undergoing transient hand-to-hand motion through the network. We develop a self-consistent theory for describing transiently associating polymer solutions that captures these complex dynamics. A single polymer chain transiently binds to a viscoelastic background that represents the polymer network formed by surrounding polymer chains. The viscoelastic background is described in the equation of motion as a memory kernel, which is self-consistently determined based on the predicted rheological behavior from the chain itself. The solution to the memory kernel is translated into rheological predictions of the complex modulus over a wide range of frequencies to capture the time-dependent behavior of a physical gel. Using the loss tangent predictions, a phase diagram is shown for the sol-gel transition of polymers with dynamic association affinities. This theory provides a predictive, molecular-level framework for the design of associating gels and supramolecular assemblies with targeted rheological properties.

DOI: [10.1103/PhysRevE.102.020501](https://doi.org/10.1103/PhysRevE.102.020501)

Polymers with dynamic associations are critical to many modern engineering applications, including stimuli-responsive materials [1], self-healable electronic devices [2], lithium-ion batteries [3], and cell culture matrices for directed stem-cell delivery and differentiation [4–7]. These polymers exhibit complex flow behavior, characterized by time-dependent stress responses to flow deformation. Such complex behavior derives from the cascade of molecular relaxation times associated with chain relaxations, entanglements, and interchain associations and interactions. Theoretical models that can fully capture the essential physics underlying these polymer networks have considerable value in predicting the performance of new materials.

An archetypal example is reptation theory for the flow behavior of highly entangled polymeric fluids and melts [8–13]. A single polymer chain within an entangled melt slithers (or reptates) back and forth within a tube defined by the surrounding polymers. Reptation theory renders concrete predictions for various properties that are in general agreement with experimental observations, though detailed comparisons reveal subtle distinctions [14]. Refinements of reptation theory generally acknowledge that the confinement tube is not a static entity by introducing physical effects such as constraint release or confinement-tube end fluctuations [15–18]. Computational realizations of entangled polymer melts as slip-link networks [10,14,19–21] result in rheological behavior that involves relaxation of the entanglements throughout the timescale of polymer relaxation.

Interchain associations that occur in dynamically crosslinked gels introduce additional relaxation processes that are not captured by the reptation mechanism. The sticky Rouse and sticky reptation models [22–25] provide valuable frameworks for interpreting the rheological behavior of associating polymer networks [26–28]. These models

describe a flexible chain (i.e., a Rouse polymer) whose associating groups experience an effective friction that scales with the bond lifetime. Thus, the underlying dynamics of the network are represented in the model as an effective Newtonian friction (i.e., no frequency dependence) that does not reflect the underlying frequency-dependent response of the viscoelastic network.

In dynamically associating networks, one imagines a single chain moving through a polymer network via a mechanism of transient reaching, grabbing, and releasing of the polymer network (see Fig. 1). This mechanism is more akin to the hand-to-hand translocation of a primate through the branches of a tree, which is dubbed *brachiation*. The network is not a static entity, and a polymer segment that is attached would experience a response that reflects the viscoelastic memory of the network.

We develop a theoretical framework to analyze the brachiating motion of a polymer chain in the presence of a dynamic network. This model captures transient associations, resulting from chemical units along the chains forming dynamic bonds that dominate the relaxation processes of the surrounding viscoelastic network. We introduce a self-consistent relationship between the single-chain dynamics and the memory kernel of the network, resulting in a predictive model for the rheological behavior whose parameters are based on experimentally measurable physical properties.

We consider a single flexible polymer chain of length N (i.e., number of Kuhn segments) containing M chemical units that exhibit transient associations with neighboring polymers. The conformation is defined by the space curve $\vec{r}(n, t)$, where n is an arc-length parameter that runs from zero at one chain end to N at the opposite end. The binding sites are equally spaced along the chain, such that the i th binding site is located at position $n_i = N(i - 1)/(M - 1)$. We neglect long-range

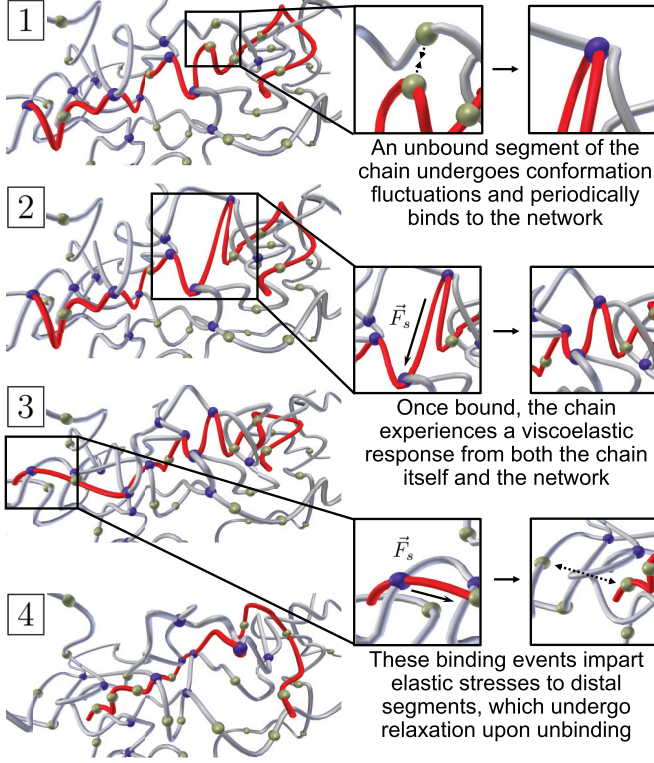


FIG. 1. Schematic representation of the brachiating motion of a polymer chain undergoing transient binding and unbinding with a dynamic network.

hydrodynamic interactions between segments of the polymer. These effects are frequently captured using a preaveraging approximation (e.g., the Zimm model) [13]. Such an approach for semidilute conditions requires further development to define a crossover from Zimm-like to Rouse-like behavior with increasing length scale [24,25]. We relegate such a treatment to future work.

The dynamic motion of the chain is governed by the Langevin equation

$$\begin{aligned} \xi \frac{\partial \vec{r}(n, t)}{\partial t} + \sum_{i=1}^M \delta(n - n_i) \int_0^t dt' K(|t - t'|) \sigma_i(t, t') \frac{\partial \vec{r}(n, t')}{\partial t} \\ = \frac{3k_B T}{b^2} \frac{\partial^2 \vec{r}(n, t)}{\partial n^2} + \vec{f}^{(B)}(n, t), \end{aligned} \quad (1)$$

where $\sigma_i(t, t')$ is a fluctuating association that indicates whether the i th segment is bound at the current time t and remains bound for all past times until t' [i.e., $\sigma_i(t, t') = 1$ if bound for all times between t' and t , and $\sigma_i(t, t') = 0$, otherwise]. Thus, the i th associating segment experiences a viscoelastic memory kernel K between t' and t only if the segment remains bound throughout that time period. The Brownian force $\vec{f}^{(B)}$ obeys the fluctuation dissipation theorem

$$\begin{aligned} \langle \vec{f}^{(B)}(n, t) \vec{f}^{(B)}(n', t') \rangle \\ = 2k_B T \xi \delta(n - n') \mathbf{I} \\ + k_B T K(|t - t'|) \sum_{i=1}^M \sigma_i(t, t') \delta(n - n_i) \delta(n' - n_i) \mathbf{I}. \end{aligned} \quad (2)$$

The kernel K represents the viscoelastic memory of the surrounding polymeric network that only influences site i during contiguous time periods of association. Thus, we assume that the site loses memory of past deformations immediately upon detachment. The exact mathematical form of K is defined through a self-consistent calculation that links the network rheology back to the single-chain dynamics. This is formally defined below.

The Langevin equation [Eq. (1)] acts as the starting point for evaluating the rheological behavior of the polymeric fluid [13]. We define the p th normal mode $\phi_p(n)$, where $\phi_p = \sqrt{2} \cos(p\pi n/N)$ for $p \neq 0$ and $\phi_0 = 1$. The chain conformation is expressed as a normal-mode expansion $\vec{r}(n, t) = \sum_{p=0}^{\infty} \phi_p(n) \vec{X}_p(t)$. The complex modulus $\hat{G}(\omega)$ of the polymeric fluid is determined from the molecular stress relaxation, which is related to the normal-mode correlation function

$$C_{pp'}(t) = \langle \vec{X}_p(t) \cdot \vec{X}_{p'}(0) \rangle. \quad (3)$$

We perform a normal-mode expansion of Eq. (1), multiply by $\vec{X}_{p'}$, and take the ensemble average (denoted by the angle brackets $\langle \dots \rangle$).

In this work, we explore the linear viscoelastic behavior of our model, based on the assumption that both the chain configurations and the binding and unbinding kinetics are governed by their equilibrium behaviors. Significant flow deformation would perturb the chain conformations, resulting in local forces that are likely to modify the instantaneous unbinding rates [29–31]. We relegate a treatment of the nonlinear viscoelastic behavior of our model to future work. We assume the binding/unbinding kinetics obeys Poisson statistics and that the rates are independent of the instantaneous forces experienced at the binding sites, resulting in the expression $\langle \sigma(t, t') \rangle = p_b \exp(-k_u |t - t'|)$. The equilibrium binding probability p_b is given by $p_b = k_b c M / (k_u + k_b c M) = K_{eq} c M / (1 + K_{eq} c M)$, where k_b and k_u are binding and unbinding rate constants, respectively, and c is the polymer-chain concentration (per unit volume). We define the equilibrium constant for binding $K_{eq} = k_b / k_u$.

We nondimensionalize all timescales by the Rouse time $\tau_R = N^2 b^2 \xi / (3\pi^2 k_B T)$, which represents the relaxation time of a single polymer in the absence of associations. The Laplace-transformed correlation function $\hat{C}_{pp'}(s)$ (i.e., from t/τ_R to s) is governed by

$$\begin{aligned} \sum_{p''=1}^{\infty} \{s \delta_{pp''} + p_b M \Phi_{pp''} s \hat{K}(s + K_u) + p^2 \delta_{pp''}\} \hat{C}_{p''p'}(s) \\ = \frac{1}{p^2} \delta_{pp'} + \frac{1}{p^2} p_b M \Phi_{pp'} \hat{K}(s + K_u). \end{aligned} \quad (4)$$

The transition to dimensionless variables results in a memory kernel $\hat{K} = \hat{K}/(N\xi)$, correlation function $\hat{C}_{pp'} = \hat{C}_{pp'} N \xi / (3k_B T \tau_R^2)$, and unbinding rate constant $K_u = \tau_R k_u$. The normal-mode coupling matrix $\Phi_{pp'}$ is

$$\Phi_{pp'} = \frac{1}{M} \sum_{i=1}^M \phi_p(n_i) \phi_{p'}(n_i), \quad (5)$$

resulting in mode coupling for a finite number of associating sites M .

The single-chain dynamics results in a prediction of the complex modulus $\tilde{G}(\omega)$ (Fourier transformed from time t to frequency ω) through the expression

$$\frac{N\tilde{G}(\omega)}{ck_B T} = i\tau_R\omega \sum_{p=1}^{\infty} p^2 \hat{C}_{pp}(i\tau_R\omega). \quad (6)$$

This expression relates the Laplace-transformed correlation function $\hat{C}_{pp}(s)$ to the Fourier-transformed complex modulus $\tilde{G}(\omega)$. The final step in our theory is to relate the rheological properties, defined by the complex modulus \tilde{G} , back to the memory kernel \hat{K} . When a site is associated with the network, we assume the site experiences a viscoelastic response that is consistent with the frequency-dependent behavior of the network. Since the network behavior is determined by the single-chain relaxation [via Eq. (6)], we define a self-consistent expression for the memory kernel, which is given by

$$\hat{K}(s) = \frac{\tau_R 6\pi a}{N\xi} \frac{\hat{G}(s)}{s} = \tilde{c} \sum_{p=1}^{\infty} p^2 \hat{C}_{pp}(s), \quad (7)$$

where a is a microscopic radius associated with the local drag of a binding site within the surrounding network, and $\tilde{c} = 2b^2ac/\pi$ is a dimensionless polymer concentration.

Equation (7) allows the prediction of the complex modulus \tilde{G} from the local viscoelastic memory kernel K , based on the assumption that local forces at the length scale of the polymer chain segments can be self-consistently related to the macroscopic viscoelastic response of the network. This approximation does not account for instantaneous forces on the chain but is analogous to a variety of approaches for describing equilibrium behavior, such as in the case of thermodynamic phase behavior of polymer solutions. Models for such phase behavior are frequently cast in a mean field where an individual polymer does not interact directly with other polymers but rather with a mean-field approximation of polymer chains. The Zimm model, one of the most effective models for describing the rheological behavior in polymers including hydrodynamic interactions, does not have polymer segments interacting directly with other segments of the chain. Instead, the polymers merely interact with an average of the hydrodynamic interactions based on a preequilibrated assumption [13]. In that sense, this treatment of the hydrodynamic interactions is akin to our treatment of the physical response of the network. Moreover, the essential feature of our model is that the communication of stress is not instantaneous in time but has temporal memory, which is a hallmark feature of viscoelastic fluids.

The numerical procedure for rendering predictions for \tilde{G} involves the following steps. First, we evaluate $\hat{C}_{pp'}(i\tau_R\omega + nK_u)$ for large n , which is approximately given by the value

$$\hat{C}_{pp'}(i\tau_R\omega + nK_u) \approx \frac{1}{nK_u + p^2} \delta_{pp'} - \frac{i\tau_R\omega}{(nK_u + p^2)^2} \delta_{pp'}. \quad (8)$$

The value of n at the starting point (n_{\max}) is selected to ensure that the first step is numerically accurate over the entire frequency range. This is achieved by evaluating $\hat{C}_{pp'}[i\tau_R\omega_{\max} + (n_{\max} - 1)K_u]$ using Eq. (4), where ω_{\max} is the maximum frequency in the range of the prediction. This

is used as the starting point for evaluating $\hat{C}_{pp'}(i\tau_R\omega + nK_u)$, since the largest frequency is the case where the asymptotic form in Eq. (8) is least accurate. We then compare the evaluated $\hat{C}_{pp'}[i\tau_R\omega_{\max} + (n_{\max} - 1)K_u]$ against the asymptotic form in Eq. (8) to ensure accuracy (within 0.01%). Then, we iteratively evaluate $\hat{C}_{pp'}(i\tau_R\omega + nK_u)$ [using Eq. (4)] from large n to $n = 0$. The resulting value of $\hat{C}_{pp'}(i\tau_R\omega)$ is used to predict the complex modulus G . Python scripts that are used to calculate G are available on the Spakowitz laboratory website.

Figure 2 provides predictions for the complex modulus $G = G' + iG''$ (black curves), where G' is the storage modulus (solid) and G'' is the loss modulus (dashed), versus the frequency $\tau_R\omega$. These plots show a range of concentration \tilde{c} and unbinding rate K_u for fixed equilibrium constant $K_{\text{eq}} = 1$. The gray curves provide predictions from the Rouse model as a reference. The vertical dashed lines indicate the value of K_u in each plot, and the crossover frequency ω_* (black dot) shows where $G' = G''$.

The complex modulus from our theory exhibits hallmark features of gelation. For large unbinding rate K_u , the release from the network is instantaneous, and the internal Rouse modes dominate the viscoelastic behavior of the solution, as can be seen from the complex modulus tending to the Rouse model for large K_u and low concentration. As the unbinding rate decreases, the chain experiences longer association times to the viscoelastic network. These associations lead to segmental motions experiencing the viscoelastic drag of the network. At timescales (i.e., inverse of frequency) where the network exhibits viscous behavior ($G'' > G'$), chain segmental motion has minimal elastic memory within the kernel K . In the low-frequency limit, the effective viscous drag of the network dominates the chain motion, resulting in a loss modulus G'' that is always larger than predictions from the Rouse model. At timescales where the network exhibits elastic behavior ($G' > G''$), chain motion is governed by both the internal Rouse modes and the elastic response of the network. In the high-frequency limit, the internal Rouse modes dominate, resulting in a convergence with the Rouse model for all conditions. The emergence of a plateau modulus indicates a broad range of timescales where the polymer network behaves effectively as an elastic solid, and the segmental motion is determined by the elastic response of the network. Moreover, the ability for these predictions to span such a broad frequency range, capturing three regimes of viscoelastic behavior, has not been achieved by previous models and demonstrates an advantage of our theory.

Though the crossover frequency ω_* shown in Fig. 2 correlates with the unbinding rate K_u , they do not exactly coincide. Figure 3 shows the crossover frequency ω_* versus the unbinding rate K_u for a range of concentrations and a fixed value of $K_{\text{eq}} = 1$. The limiting behavior as $K_u \rightarrow 0$ scales as $\omega_* \sim K_u$, shown in Fig. 3 as the dotted curves. However, the theory deviates significantly from this trend with increasing K_u , particularly as $K_u \gg 1$. In this limit, the unbinding rate K_u is sufficiently fast that the gel is no longer stable, marking the transition to the solution phase (i.e., the sol phase). In the gel phase, the viscoelastic response of the network dominates the relaxation behavior of a polymer chain, and the sol phase arises when the internal Rouse modes dominate the behavior. The polymer concentration modulates the crossover between

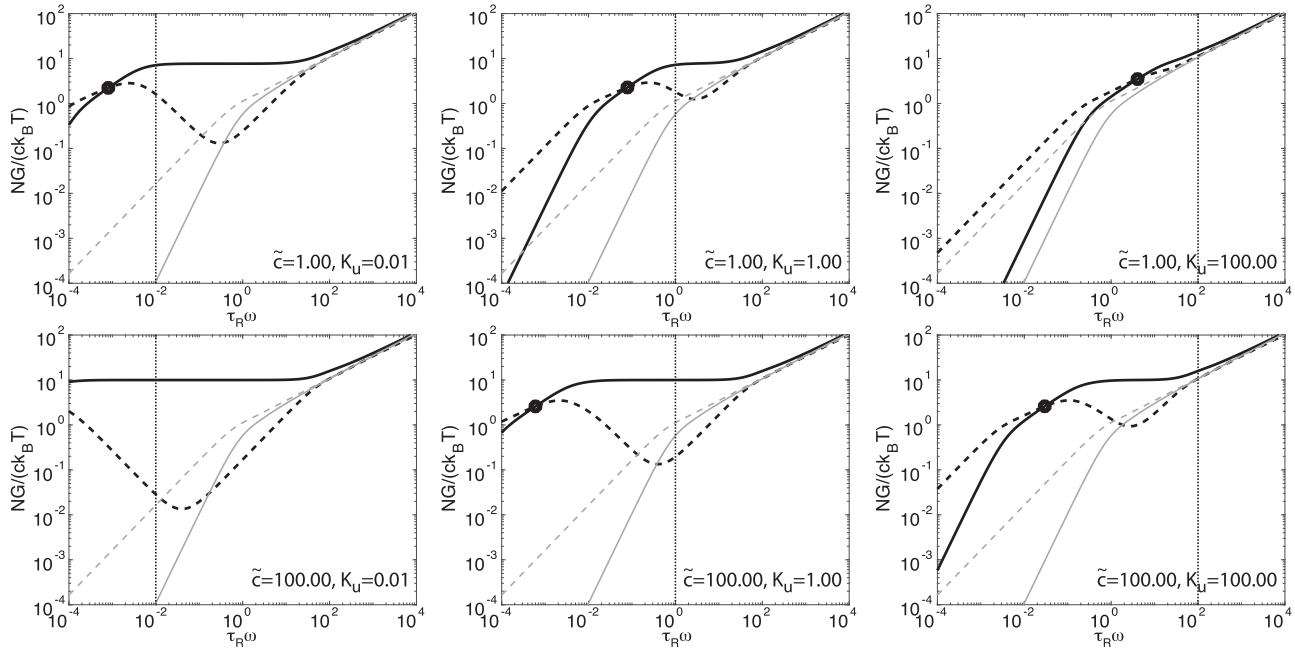


FIG. 2. Theoretical predictions for the storage modulus G' (solid) and loss modulus G'' (dashed) versus the frequency $\tau_R\omega$, where τ_R is the Rouse time of the polymer. The black curves are based on our theory, and the gray curves show predictions from the Rouse model. Predictions are shown over a range concentration \tilde{c} and unbinding rate K_u for a fixed value of $K_{eq} = 1$. The black dot identifies the crossover frequency ω_* , and the vertical dotted line indicates the unbinding rate K_u .

gel and sol phases (demonstrated in Fig. 3 by the points where the solid line deviates from the dotted line for each concentration). Increasing concentration \tilde{c} leads to increased crosslink density and elasticity of the network, which decreases the crossover frequency ω_* since a more elastic network requires a longer time to relax. Similarly, increased elasticity due to higher concentration \tilde{c} requires faster unbinding rate K_u of the associations to cross over from the gel to the sol phase.

A sol-gel phase diagram over a range of polymer concentration \tilde{c} and equilibrium constant K_{eq} (fixed unbinding rate $K_u = 1$) is provided in Fig. 4. In the inset plot of $\tan \delta = G''/G'$ versus frequency, we define the emergence of a minimum between the curves for $\tilde{c} = 0.10$ and $\tilde{c} = 1.00$ as the transition between the sol and gel phase. The phase diagram in the main plot is constructed by identifying this transition over the range of K_{eq} values.

Two regimes are present in the phase diagram. For low K_{eq} values, sufficient polymer concentration is needed for adequate binding probability p_b to engage the network and

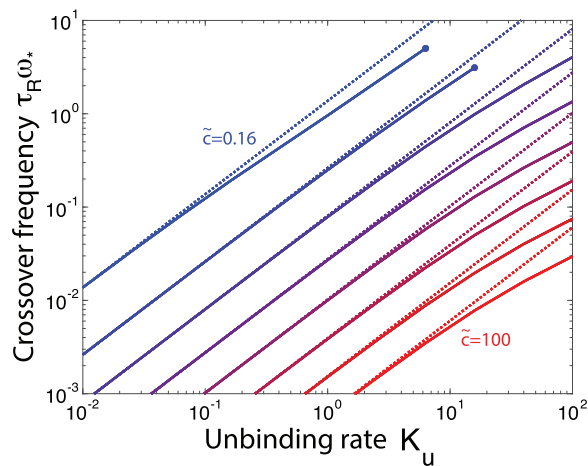


FIG. 3. Crossover frequency ω_* versus unbinding rate constant K_u over a range of concentrations from $\tilde{c} = 0.16$ to $\tilde{c} = 100$ for a fixed value of $K_{eq} = 1$. The dotted curves indicate a linear power law $\omega_* \sim K_u$, which is valid as $K_u \rightarrow 0$. The value of the crossover frequency ω_* and the unbinding rate constant K_u where the dotted and solid lines deviate as a function of polymer concentration \tilde{c} indicate the significant influence of concentration on the sol-gel transition.

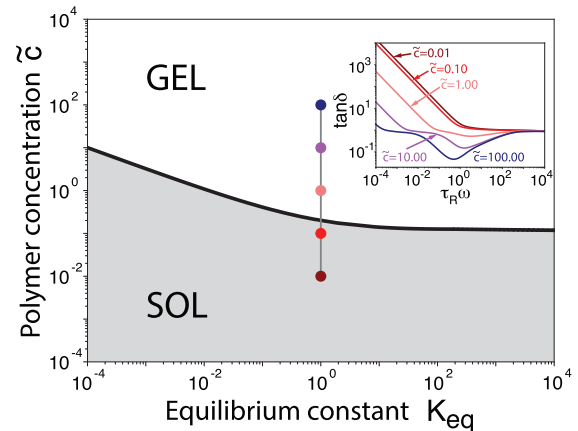


FIG. 4. The inset plot shows $\tan \delta = G''/G'$ versus frequency ω over a range of concentrations \tilde{c} and fixed $K_{eq} = 1$ and $K_u = 1$. The main plot shows the sol-gel phase diagram for concentration \tilde{c} and equilibrium constant K_{eq} at a fixed unbinding constant $K_u = 1$. The dots indicate the conditions coinciding with the inset plot of $\tan \delta$.

sustain an elastic plateau that marks gelation. The scaling of the gelation concentration in this regime is $\tilde{c}_{\text{gel}} \sim K_{\text{eq}}^{-1/2}$. The second regime occurs at large K_{eq} values (i.e., $K_{\text{eq}} \gg 1$). Here, the binding probability $p_b \approx 1$ for any modest polymer concentration ($\tilde{c} \approx 1$). However, binding does not imply adequate viscoelastic traction for a plateau modulus to emerge, and the chain dynamics are dominated by internal Rouse modes rather than network viscoelasticity. In this regime, the gelation concentration tends to a constant.

Our rheological model establishes a predictive framework based on molecular physics. Rheological data is frequently modeled using phenomenological constitutive equations (e.g., the Maxwell model) [32], which may have molecular inspiration but do not easily guide molecular design. In contrast, our model has the ability to make rheological predictions that can be leveraged for the rational design of new supramolecular materials [33]. Importantly, all of the input parameters for our model directly correlate to experimentally measurable quantities (i.e., unbinding rate, equilibrium constant, concentration). For example, transient associations may be formed by reversible covalent bonds, for which the binding and unbinding rates can be found via high-performance liquid chromatography [34].

The need for a predictive tool in material design is especially relevant in the areas of drug delivery and tissue engineering. Supramolecular materials have long been leveraged for slow-release drug applications and continue to be utilized for more advanced drug delivery functions, such as biopolymers designed to display growth factor binding affinity in order to stimulate blood vessel growth [35]. Polymer materials with dynamic associations are also leveraged in synthesizing mimics of the natural extracellular matrix, where material stiffness, stress relaxation, and composition influence cell behavior and stem cell fate [36,37]. Despite the large body of materials available to experimentalists, the ideal cell culture scaffold and drug delivery vehicle has yet to be found [5], and most experimentalists heavily rely on trial and error to achieve the desired material properties. Although there exist

decades of theoretical models to describe polymer networks, these phenomenological models, while exhibiting reasonable fits to experimental data, aim to describe aspects of the bulk behavior while eschewing molecular detail, hindering a molecular-level approach for material design.

Transient associations imply periodic engagement of the chain with the dynamic network. Thus, the chain's fluctuating conformation is akin to the motion of a primate through a jungle, where translation occurs through the transient passing of the primate through the tree branches in a hand-to-hand manner. The engagement of a hand to a branch does not imply the branch is static, rather the branch would move in concert with (or in physical response to) the motion of the body.

Similarly, the transient association of a polymer segment to the network results in the segment experiencing a local temporal response that mimics the relaxation processes of the surrounding dynamic network. Our approach introduces a self-consistent realization of this frequency dependence rather than resorting to an ad hoc definition or a fitting procedure. This places an emphasis on the chain dynamics defining the effective medium, and the resulting frequency dependence of the polymeric fluid dramatically influences the chain motion, which has been implicated in the modeling of biopolymers such as DNA in living cells [38–40]. Furthermore, many complex fluids and materials, including glasses and colloidal gels, exhibit mechanical responses with temporal memory, and our approach provides an avenue to predict their collective dynamics. Finally, we envision this approach would be valuable for a range of polymeric problems, particularly in the semidilute regime where chain interactions cannot be approximated as a static confinement.

We greatly appreciate discussions with David Morse, Ronald Larson, Jay Schieber, and Jian Qin during the development of this work. Financial support is provided by the National Science Foundation (NSF), Physics of Living Systems Program (PHY-1707751).

-
- [1] R. J. Wojtecki, M. A. Meador, and S. J. Rowan, *Nat. Mater.* **10**, 14 (2011).
- [2] J. Kang, J. B.-H. Tok, and Z. Bao, *Nat. Electronics* **2**, 144 (2019).
- [3] C. Wang, H. Wu, Z. Chen, M. T. McDowell, Y. Cui, and Z. Bao, *Nat. Chem.* **5**, 1042 (2013).
- [4] C. T. W. P. Foo, J. S. Lee, W. Mulyasmita, A. Parisi-Amon, and S. C. Heilshorn, *Proc. Natl. Acad. Sci. USA* **106**, 22067 (2009).
- [5] H. Wang and S. C. Heilshorn, *Adv. Mater.* **27**, 3717 (2015).
- [6] O. Chaudhuri, L. Gu, D. Klumpers, M. Darnell, S. A. Bencherif, J. C. Weaver, N. Huebsch, H.-P. Lee, E. Lippens, G. N. Duda *et al.*, *Nat. Mater.* **15**, 326 (2016).
- [7] G. A. Roth, E. C. Gale, M. Alcántara-Hernández, W. Luo, E. Axpe, R. Verma, Q. Yin, A. C. Yu, H. L. Hernandez, C. L. Maikawa, A. A. A. Smith, M. M. Davis, B. Pulendran, J. Idoyaga, and E. A. Appel, *bioRxiv* (2020), doi: 10.1101/2020.05.26.117465.
- [8] P.-G. de Gennes, *J. Chem. Phys.* **55**, 572 (1971).
- [9] M. Doi and S. F. Edwards, *J. Chem. Soc. Faraday Trans. II* **74**, 1789 (1978).
- [10] M. Doi and S. F. Edwards, *J. Chem. Soc. Faraday Trans. II* **74**, 1802 (1978).
- [11] M. Doi and S. F. Edwards, *J. Chem. Soc. Faraday Trans. II* **74**, 1818 (1978).
- [12] M. Doi and S. F. Edwards, *J. Chem. Soc. Faraday Trans. II* **75**, 38 (1979).
- [13] M. Doi and S. F. Edwards, *The Theory of Polymer Dynamics* (Oxford University Press, New York, 1988), Vol. 73.
- [14] C. C. Hua and J. D. Schieber, *J. Chem. Phys.* **109**, 10018 (1998).
- [15] W. W. Graessley, *Synthesis and Degradation Rheology and Extrusion* (Springer, New York, 1982), pp. 67–117.
- [16] S. T. Milner and T. C. B. McLeish, *Phys. Rev. Lett.* **81**, 725 (1998).
- [17] H. Watanabe, *Prog. Polym. Sci.* **24**, 1253 (1999).

- [18] T. McLeish, *Adv. Phys.* **51**, 1379 (2002).
- [19] C. C. Hua, J. D. Schieber, and D. C. Venerus, *J. Chem. Phys.* **109**, 10028 (1998).
- [20] C. C. Hua, J. D. Schieber, and D. C. Venerus, *J. Rheol.* **43**, 701 (1999).
- [21] A. Kushwaha and E. S. Shaqfeh, *J. Rheol.* **55**, 463 (2011).
- [22] L. Leibler, M. Rubinstein, and R. H. Colby, *Macromolecules* **24**, 4701 (1991).
- [23] A. N. Semenov and M. Rubinstein, *Macromolecules* **31**, 1373 (1998).
- [24] M. Rubinstein and A. N. Semenov, *Macromolecules* **31**, 1386 (1998).
- [25] M. Rubinstein and A. N. Semenov, *Macromolecules* **34**, 1058 (2001).
- [26] Q. Chen, G. J. Tudryn, and R. H. Colby, *J. Rheol.* **57**, 1441 (2013).
- [27] S. Tang, M. Wang, and B. D. Olsen, *J. Am. Chem. Soc.* **137**, 3946 (2015).
- [28] D. Xu and S. L. Craig, *Macromolecules* **44**, 5465 (2011).
- [29] E. Evans, *Annu. Rev. Biophys. Biomol. Struct.* **30**, 105 (2001).
- [30] A. P. Wiita, S. R. K. Ainarapu, H. H. Huang, and J. M. Fernandez, *Proc. Natl. Acad. Sci. USA* **103**, 7222 (2006).
- [31] E. F. Koslover and A. J. Spakowitz, *Phys. Rev. E* **86**, 011906 (2012).
- [32] C. W. Macosko, *Rheology: Principles, Measurements, and Applications* (Wiley-VCH, 1994).
- [33] E. A. Appel, F. Biedermann, U. Rauwald, S. T. Jones, J. M. Zayed, and O. A. Scherman, *J. Am. Chem. Soc.* **132**, 14251 (2010).
- [34] J. Lou, F. Liu, C. D. Lindsay, O. Chaudhuri, S. C. Heilshorn, and Y. Xia, *Adv. Mater.* **30**, 1705215 (2018).
- [35] M. J. Webber and R. Langer, *Chem. Soc. Rev.* **46**, 6600 (2017).
- [36] O. Chaudhuri, S. T. Koshy, C. B. Da Cunha, J.-W. Shin, C. S. Verbeke, K. H. Allison, and D. J. Mooney, *Nat. Mater.* **13**, 970 (2014).
- [37] O. Chaudhuri, L. Gu, M. Darnell, D. Klumpers, S. A. Bencherif, J. C. Weaver, N. Huebsch, and D. J. Mooney, *Nat. Commun.* **6**, 6365 (2015).
- [38] S. C. Weber, A. J. Spakowitz, and J. A. Theriot, *Phys. Rev. Lett.* **104**, 238102 (2010).
- [39] S. C. Weber, J. A. Theriot, and A. J. Spakowitz, *Phys. Rev. E* **82**, 011913 (2010).
- [40] S. C. Weber, A. J. Spakowitz, and J. A. Theriot, *Proc. Natl. Acad. Sci. USA* **109**, 7338 (2012).